

The Generalized Nonlinear Ohm's Law: How a Strong Electric Field Influences Non-ideal MHD Effects in Dusty Protoplanetary Disks

SATOSHI OKUZUMI,¹ SHOJI MORI,^{1,2} AND SHU-ICHIRO INUTSUKA³¹*Department of Earth and Planetary Sciences, Tokyo Institute of Technology, Meguro-ku, Tokyo 152-8551, Japan*²*Department of Astronomy, The University of Tokyo, Bunkyo-ku, Tokyo 113-0033, Japan*³*Department of Physics, Nagoya University, Nagoya, Aichi 464-8602, Japan*

ABSTRACT

The magnetohydrodynamics (MHD) of protoplanetary disks are strongly subject to the non-ideal MHD effects arising from the low ionization fraction of the disk gas. A strong electric field induced by gas motions can heat ionized gas particles and can thereby affect the ionization balance in the disks. Our previous studies revealed that in dusty protoplanetary disks, the Ohmic conductivity decreases with increasing electric field strength until the electrical breakdown of the disk gas occurs. In this study, we extend our previous work to more general cases where both electric and magnetic fields affect the motion of plasma particles, allowing us to study the impacts of plasma heating on all non-ideal MHD effects: Ohmic, Hall, and ambipolar diffusion. We find that the upper limit on the electric current we previously derived applies even in the presence of magnetic fields. Although the Hall and ambipolar resistivities can either increase or decrease with electric field strength depending on the abundance of charged dust grains, the Ohmic resistivity always increases with electric field strength. An order-of-magnitude estimate suggests that a large-scale electric current generated by gas motions in the inner part of protoplanetary disks could exceed the upper limit. This implies that MHD motions of the inner disk, such as the motion driven by the Hall-shear instability, could either get suppressed or trigger electrical breakdown (lightning discharge). This may have important implications for gas accretion and chondrule formation in the inner part of protoplanetary disks.

Keywords: accretion, accretion disks — instabilities — magnetohydrodynamics (MHD) — planets and satellites: formation — plasmas — protoplanetary disks — turbulence

1. INTRODUCTION

The dynamics and evolution of protoplanetary disks is key to understanding formation occurring in the disks. Like in many astrophysical systems, magnetic field is thought to play an important role in the gas dynamics in the disks.

However, because the interior of protoplanetary disks is poorly ionized, the MHD of the disks is strongly subject to the effects arising from the finite electrical conductivities of the gas, the so-called non-ideal MHD effects (see [Turner et al. 2014](#) for a review). It has long been recognized that Ohmic diffusion stabilizes the magnetorotational instability (MRI; [Balbus & Hawley 1991](#)) in the dense, cool part of the disks (e.g., [Gammie 1996](#); [Sano et al. 2000](#)). However, Ohmic diffusion is the dominant non-ideal MHD effect only when the gas drag acting on the plasma particles is stronger

than the magnetic Lorentz force acting on them, which is only the case in the inner part of the disks ([Kunz & Balbus 2004](#); [Wardle 2007](#); [Bai 2011](#)). In fact, recent MHD simulations have shown that ambipolar diffusion, another non-ideal MHD effect, substantially damps the MRI on the surface and in the outer part of the disks ([Bai & Stone 2013a](#); [Simon et al. 2013a,b](#); [Gressel et al. 2015](#)). The Hall drift, the last non-ideal MHD effect, further changes the disk dynamics by introducing the Hall-shear instability (HSI) to disks whose net vertical magnetic field has the same direction as the disk rotation vector ([Kunz 2008](#); [Wardle & Salmeron 2012](#)). The Hall-shear instability amplifies horizontal magnetic fields, thus allowing for accretion in the relatively inner part of the disk ([Bai 2014, 2015, 2017](#); [Lesur et al. 2014](#)). Thus, it is essential to fully understand the conductivity of gas in protoplanetary disks.

Conventionally, models of disk ionization in protoplanetary disks (e.g., [Sano et al. 2000](#); [Ilgner & Nelson 2006](#); [Wardle 2007](#); [Bai & Goodman 2009](#); [Okuzumi 2009](#)) assume that the ionization state is determined by the balance be-

tween external ionization and recombination of plasma particles within the gas and on dust grains. It is also assumed implicitly that the electric field as measured in the comoving frame of the gas, which drives electric current in the disk, is so weak that it has no effect on the plasma temperatures. However, because the gas disk is poorly conducting, the electric field accompanied by the MHD motions of the disks can be strong, potentially affecting the plasma temperatures and even the ionization balance. Inutsuka & Sano (2005) first pointed out that the electric field inside MRI-driven turbulence could be strong enough to cause electrical breakdown of the disk gas, potentially leading to self-sustained turbulence in which the high electric conductivity provided by the breakdown keeps the MRI active without additional ionizing sources. This self-sustaining mechanism for the MRI in protoplanetary disks was later confirmed by Muranushi et al. (2012), who performed MHD simulations in which the Ohmic conductivity was allowed to increase arbitrarily at a certain electric field strength to mimic electrical breakdown.

More recently, Okuzumi & Inutsuka (2015, henceforth *Paper I*) developed a charge reaction model that incorporates plasma heating by electric field, showing that plasma heating does not only enhance but can also suppress the conductivity of disk gas. They found that as plasma particles are electrically heated, they collide with and stick onto dust grains more frequently, and consequently the plasma densities in the gas decrease. The decrease in the conductivity with increasing electric field strength gives rise to an upper limit on the electric current that can only be exceeded with electrical breakdown. This effect could quench MHD turbulence before the electric field strength reaches the breakdown threshold (Mori & Okuzumi 2016; Mori et al. 2017). The upper limit on the plasma current can also facilitate charge separation and even lead to lightning discharge. (Johansen & Okuzumi 2018) recently propose that this lightning discharge might have led to the formation of chondrules, millimeter-sized solid particles that experienced melting by flash heating events, found in meteorites (see, e.g., Whipple 1966; Desch & Cuzzi 2000, for the lightning scenario for chondrule formation).

There are two important limitations to the formulation of *Paper I*. Firstly, we assumed that collisions between electrons and neutrals are purely elastic. This assumption is valid at low electric field strengths where electron heating starts to be effective, but breaks down once the electron energy exceeds the excitation energies of neutrals. By neglecting inelastic energy losses, we overestimated the electron energy at high electric field strengths. Secondly, we neglected the effects of magnetic fields on the motion of plasma particles by assuming that the gas drag force acting on the particles is stronger than the magnetic Lorentz force. For this reason, the previous model is not able to treat Hall drift and ambipolar diffusion, and therefore inapplicable to the dense inner part

of the disks where these non-Ohmic effects dominate. The purpose of this paper is to reformulate the work of *Paper I* and provide a model that can treat all non-ideal MHD effects as well as non-elastic plasma–neutral collisions.

This paper is organized as follows. In Section 2, we formulate the kinetics of charged gas particles in the presence of both electric and magnetic fields and illustrate how magnetic fields as well as inelastic energy losses affect the electric heating of plasmas. This kinetic model is used in Sections 3 to present analytic estimates of the electric current at high electric field strengths in the presence of magnetic fields. In Section 4, we combine the kinetic model with a simplified charge reaction model to demonstrate how the electric current and magnetic resistivities depend on the magnitude and direction of an applied electric field. Implications for the MHD of protoplanetary disks are discussed in Section 5, and a summary is presented in Section 6.

2. KINETICS OF WEAKLY IONIZED PLASMAS IN ELECTRIC AND MAGNETIC FIELDS

We begin by studying how the presence of magnetic field affects electric heating of plasmas in a neutral gas. In *Paper I*, we calculated the electron kinetic energy and other related quantities directly from the exact velocity distribution function for electrons. Such an approach is rigorous, but is useful only when a simple and closed analytic expression for the velocity distribution is known. The electron velocity distribution adopted in *Paper I*, the so-called Davydov distribution (Davydov 1935), is only valid when the electron–neutral collisions are purely elastic and when no magnetic field is present. Unfortunately, there is no known exact expression for the electron velocity distribution for more general cases.

In this study, we use an alternative approach based on the moment formalism (Golant et al. 1980). In this approach, we approximate the velocity distribution functions of ions and electrons with a Maxwellian whose center is offset in the velocity space. This offset Maxwellian distribution is characterized by the mean velocity and mean energy of the plasma particles, which we determine by solving the first and second moment equations of the Boltzmann equation including the magnetic Lorentz force. This way, we are able to compute the mean and random velocities of a plasma in the presence of both magnetic and electric field without having to solve the original Boltzmann equation numerically. In *Paper I*, we already applied this approach to ions, whose velocity distribution has no exact analytic expression even in the absence of magnetic field (Wannier 1953). In this study, we apply this approach to both ions and electrons.

2.1. Moment Equations for the Drift Velocities and Mean Energies

We denote the velocity of plasma particles (ions and electrons) relative to the neutral gas by \mathbf{v}_α and their velocity dis-

tribution function by $f_\alpha(\mathbf{v}_\alpha)$, where $\alpha = e$ for electrons and $\alpha = i$ for ions. The mean drift velocity and mean energy, $\langle \mathbf{v}_\alpha \rangle$ and $\langle \epsilon_\alpha \rangle$, are defined as

$$\langle \mathbf{v}_\alpha \rangle \equiv \int \mathbf{v}_\alpha f_\alpha(\mathbf{v}_\alpha) d^3 v_\alpha, \quad (1)$$

$$\langle \epsilon_\alpha \rangle \equiv \frac{m_\alpha}{2} \int v_\alpha^2 f_\alpha(\mathbf{v}_\alpha) d^3 v_\alpha, \quad (2)$$

respectively, where m_α is the particle mass and $v_\alpha = |\mathbf{v}_\alpha|$.

We consider the motion of plasma particles in a neutral gas with electric and magnetic fields. If the plasma density is much lower than the neutral gas density, the motion is determined by the Lorentz force and drag force arising from the collisions with the neutrals. In the reference frame where the mean velocity of the neutrals vanishes, the first and second moments of the Boltzmann equation for plasma particles are given by (Golant et al. 1980, Chapters 6 and 9)

$$m_\alpha \frac{d\langle \mathbf{v}_\alpha \rangle}{dt} = q_\alpha \left(\mathbf{E}' + \frac{\langle \mathbf{v}_\alpha \rangle}{c} \times \mathbf{B} \right) - \mu_{\alpha n} \nu_{\alpha n} \langle \mathbf{v}_\alpha \rangle, \quad (3)$$

$$\frac{d\langle \epsilon_\alpha \rangle}{dt} = q_\alpha \mathbf{E}' \cdot \langle \mathbf{v}_\alpha \rangle - \kappa_{\alpha n} \nu_{\alpha n} \left(\langle \epsilon_\alpha \rangle - \frac{3k_B T}{2} \right), \quad (4)$$

respectively. Here, \mathbf{E}' and \mathbf{B} are the electric and magnetic fields as measured in the neutral-rest frame, respectively; c is the speed of light; q_α is the particle charge; $\mu_{\alpha n} = m_\alpha m_n / (m_\alpha + m_n)$, $\nu_{\alpha n}$, and $\kappa_{\alpha n}$ are the reduced mass, mean collision frequency, and mean energy transfer efficiency for the collision with the neutrals, respectively; k_B is the Boltzmann constant; and T is the temperature of the neutral gas. In the right-hand sides of Equations (3) and (4), the first terms represent the mean Lorentz force and mean work done by the electric field, respectively, whereas the second terms represent the mean momentum and energy losses due to the collisions with the neutrals. The prime in \mathbf{E}' emphasizes that it is the electric field in the neutral-rest frame; in the frame where the neutral gas has a mean velocity \mathbf{u} , the electric field is given by $\mathbf{E} = \mathbf{E}' - \mathbf{u} \times \mathbf{B}/c$.

2.2. Offset Maxwell Distribution Function

As stated earlier, we approximate $f_\alpha(\mathbf{v}_\alpha)$ by the offset Maxwell distribution (Hershey 1939; Paper I)

$$f_\alpha(\mathbf{v}_\alpha) = \left(\frac{m_\alpha}{2\pi k_B T_\alpha} \right)^{3/2} \exp \left(-\frac{m_\alpha (\mathbf{v}_\alpha - \langle \mathbf{v}_\alpha \rangle)^2}{2k_B T_\alpha} \right). \quad (5)$$

Here, the temperature T_α measures the kinetic energy of random motion, related to $\langle \mathbf{v}_\alpha \rangle$ and $\langle \epsilon_\alpha \rangle$ as

$$\frac{3}{2} k_B T_\alpha \equiv \langle \epsilon_\alpha \rangle - \frac{1}{2} m_\alpha \langle \mathbf{v}_\alpha \rangle^2, \quad (6)$$

It can be easily checked that $\langle \mathbf{v}_\alpha \rangle$ and $\langle \epsilon_\alpha \rangle$ in Equation (5) satisfy their definitions, Equations (1) and (2).

For electrons, the velocity distribution in a weakly ionized gas tends to be nearly isotropic, i.e., $|\langle \mathbf{v}_e \rangle| \ll \sqrt{k_B T_e / m_e}$, because of $m_e \ll m_n$ (see Golant et al. 1980, Section 5.2). Therefore, we may approximate f_e to first order in $\langle \mathbf{v}_e \rangle$ to obtain a simpler expression

$$f_e(\mathbf{v}_e) = \left(\frac{m_e}{2\pi k_B T_e} \right)^{3/2} \left(1 + \frac{m_e \mathbf{v}_e \cdot \langle \mathbf{v}_e \rangle}{k_B T_e} \right) \exp \left(-\frac{\epsilon_e^2}{k_B T_e} \right) \quad (7)$$

with

$$\frac{3}{2} k_B T_e = \langle \epsilon_e \rangle. \quad (8)$$

We will use these expressions for electrons instead of using Equations (5) and (6). We will also use that, to zeroth order in $\langle \mathbf{v}_e \rangle$, the electron speed $v_e = |\mathbf{v}_e|$ has a mean value

$$\langle v_e \rangle \approx \sqrt{\frac{8k_B T_e}{\pi m_e}} = 4 \sqrt{\frac{\langle \epsilon_e \rangle}{3\pi m_e}}. \quad (9)$$

2.3. Collision Frequencies and Energy Transfer Efficiencies

In principle, the collision frequencies $\nu_{\alpha n}$ and energy transfer efficiencies $\kappa_{\alpha n}$ are the sums of the contributions from elastic and inelastic collisions. Elastic collisions conserve the kinetic energy of the relative motion between the colliding charged and neutral particles¹, whereas inelastic collisions do not because of excitation and ionization energy losses.

In practice, the contributions of inelastic collisions are negligible for ions because the cross section for the inelastic collisions is small as long as $\epsilon_i \lesssim 10$ eV (e.g., Golant et al. 1980, Chapter 2.9). Neglecting the inelastic collisions, ν_{in} and κ_{in} are given by (e.g., Golant et al. 1980, Chapter 2)

$$\nu_{in} = K_{in} n_n, \quad (10)$$

$$\kappa_{in} = \frac{2m_i m_n}{(m_i + m_n)^2}, \quad (11)$$

respectively. Here, K_{in} is the momentum transfer rate coefficient for (elastic) ion-neutral collisions, which is independent of ion-neutral collision velocity because of the polarization force acting between them (see, e.g., Wannier 1953). We take $K_{in} = 1.6 \times 10^{-9} \text{ cm}^3 \text{ s}^{-1}$ following Nakano & Umebayashi (1986).

For electrons, the contribution of inelastic collisions is negligible to ν_{en} (but not to κ_{en} as we discuss later). Approximating f_e by a Maxwellian with $\langle \mathbf{v}_e \rangle \approx 0$, ν_{en} can formally be written as (Golant et al. 1980, Section 6.3)

$$\nu_{en} = n_n \frac{\langle \sigma_{en} v_e^3 \rangle}{\langle v_e^2 \rangle}, \quad (12)$$

¹ Note, however, that the kinetic energy of the charged particles as measured in the *neutral-rest* frame does decrease through elastic collisions. This is the reason why elastic collisions contribute to $\kappa_{\alpha n}$.

where σ_{en} is the momentum transfer cross section for electron–neutral collisions. Since σ_{en} is almost constant ($\approx 10^{-15} \text{ cm}^2$) as long as $\epsilon_e \ll 10 \text{ eV}$ (see, e.g., Figure 5 of Yoon et al. 2008), we may approximate v_{en} as

$$v_{en} = \frac{4n_n\sigma_{en}}{3}\langle v_e \rangle = \frac{16n_n\sigma_{en}}{3}\sqrt{\frac{\langle \epsilon_e \rangle}{3\pi m_e}}, \quad (13)$$

where we have used that $\langle v_e^3 \rangle / \langle v_e^2 \rangle = 4\langle v_e \rangle / 3$ under the Maxwellian approximation.

In Paper I, we neglected inelastic contributions to κ_{en} and used the expression for purely elastic collisions, $\kappa_{en} = 2m_e m_n / (m_e + m_n)^2 \approx 2m_e / m_n$. In reality, the inelastic contributions are not always negligible since the elastic contribution $\approx 2m_e / m_n$ is also small. To account for the inelastic losses, we express κ_{en} as

$$\kappa_{en} = \frac{1}{P_\ell} \frac{2m_e}{m_n}, \quad (14)$$

where P_ℓ is a dimensionless factor depending on the mean electron kinetic energy $\langle \epsilon_e \rangle$. The factor P_ℓ stands for the fractional contribution of elastic collisions to the total collisional energy loss of electrons, with $P_\ell = 1$ if the electron–neutral collisions are purely elastic and $P_\ell < 1$ otherwise. Based on the results of theoretical calculations for electron–H₂ collisions (see Appendix A), we evaluate P_ℓ as

$$P_\ell = \left(1 + \frac{\langle \epsilon_e \rangle}{0.0075 \text{ eV}}\right)^{-1/2}. \quad (15)$$

This expression reproduces theoretical estimates for P_ℓ to within a factor of 2 as long as $k_B T \lesssim 5 \text{ eV}$; for higher electron energies, (15) could underestimate energy losses due to electronic excitation and ionization (see Appendix A for details). According to Equation (15), the collisions can be regarded as elastic ($P_\ell \approx 1$) only when $\langle \epsilon_e \rangle \ll 0.01 \text{ eV}$.

2.4. Steady State Solution and the Effective and Critical Field Strengths

Since plasma particles in protoplanetary disks frequently collide with neutrals, we may assume that the velocity distribution functions for the plasmas are in steady state on the dynamical timescale of the disks. Below we derive the steady solutions of the moment equations.

Equation (3) is the basic equation for the standard generalized Ohm’s law, and its steady-state solution is already known to be (e.g., Nakano & Umebayashi 1986)

$$\langle \mathbf{v}_a \rangle = \frac{q_a}{\mu_{an} v_{an}} \left(\mathbf{E}'_{\parallel} - \frac{\beta_a}{1 + \beta_a^2} \hat{\mathbf{B}} \times \mathbf{E}'_{\perp} + \frac{\mathbf{E}'_{\perp}}{1 + \beta_a^2} \right), \quad (16)$$

where \mathbf{E}'_{\parallel} and \mathbf{E}'_{\perp} are the components of \mathbf{E}' parallel and perpendicular to \mathbf{B} , respectively, $\hat{\mathbf{B}}$ is the unit vector of \mathbf{B} , and β_a is the Hall parameter defined by

$$\beta_a = \frac{q_a B}{\mu_{an} v_{an} c} \quad (17)$$

with $B \equiv |\mathbf{B}|$. The magnitude of the Hall parameter measures the relative importance of the magnetic Lorentz force to the neutral drag force (see, e.g., Wardle & Ng 1999). If $|\beta_a| \ll 1$, the magnetic Lorentz force is negligible, the regime considered in Paper I. In general, one has $|\beta_e|/\beta_i \approx 440(T_e/300 \text{ K})^{-1/2}$, independent of B and n_n (Wardle 2007).

Substituting Equation (16) into Equation (4) and taking $d\langle \epsilon_a \rangle / dt = 0$, obtain an equation that determines $\langle \epsilon_a \rangle$ for steady state,

$$\frac{q_a^2}{\mu_{an} v_{an}} E_{\text{eff},a}^{\prime 2} - \kappa_{an} v_{an} \left(\langle \epsilon_a \rangle - \frac{3k_B T}{2} \right) = 0, \quad (18)$$

where we have introduced the effective electric field strength for charged species α (Golant et al. 1980, Chapter 5),

$$E'_{\text{eff},\alpha} \equiv \sqrt{E_{\parallel}^{\prime 2} + \frac{E_{\perp}^{\prime 2}}{1 + \beta_{\alpha}^2}}, \quad (19)$$

with $E'_{\parallel} \equiv |\mathbf{E}'_{\parallel}|$ and $E'_{\perp} \equiv |\mathbf{E}'_{\perp}|$. Equation (18) is key to understanding how magnetic fields affect the electric heating of plasmas. It is $E'_{\text{eff},\alpha}$, not the magnitude of the total electric field $E' = (E_{\parallel}^{\prime 2} + E_{\perp}^{\prime 2})^{1/2}$, that determines the rate of plasma heating (the first term in Equation (18)) in the presence of a magnetic field. Because $E'_{\text{eff},\alpha} \leq E'$, magnetic fields generally suppress the plasma heating. In particular, when $\mathbf{E}' \perp \mathbf{B}$ (i.e., $E'_{\parallel} = 0$ and $E'_{\perp} = E'$) and $|\beta_a| \gg 1$, $E'_{\text{eff},\alpha}$ is smaller than E' by a factor of $1/|\beta_a| \ll 1$.

For ions, v_{in} is independent of $\langle \epsilon_i \rangle$, and hence Equation (18) can be analytically solved as

$$\langle \epsilon_i \rangle = \frac{3}{2} k_B T + \frac{e^2}{\mu_{in} \kappa_{in} v_{in}^2} E_{\text{eff},i}^{\prime 2}. \quad (20)$$

In the right-hand side of Equation (20), the first term indicates that the ion temperature is equal to the neutral temperature in the absence of electric fields. The second term represents ion heating by the electric field, and is larger than the first term when $E_{\text{eff},i}$ is above the threshold

$$E_{\text{crit},i} \equiv \frac{v_{in}}{e} \sqrt{\frac{3\mu_{in} \kappa_{in} k_B T}{2}} \approx \frac{m_n n_n K_{in}}{e} \sqrt{\frac{3k_B T}{m_i}}. \quad (21)$$

In the final expression, where we have used that $m_i \gg m_n$.

For electrons, Equation (18) with Equations (13)–(15) is a transcendental equation for $\langle \epsilon_e \rangle$, which we must solve numerically. It is useful to note, however, that Equation (18) can formally be rewritten as

$$\langle \epsilon_e \rangle = \frac{3}{2} k_B T \left(\frac{1}{2} + \frac{1}{2} \sqrt{1 + \frac{9\pi P_\ell}{16} \left(\frac{E'_{\text{eff},e}}{E_{\text{crit},e}} \right)^2} \right), \quad (22)$$

where

$$E_{\text{crit},e} \equiv \sqrt{\frac{6m_e}{m_n} \frac{n_n \sigma_{en} k_B T}{e}} \quad (23)$$

is the critical field strength for electron heating introduced in Paper I.² Equation (22) suggests that electron heating occurs at $E'_{\text{eff},e} \geq E_{\text{crit},e} / \sqrt{P_\ell}$. Since $P_\ell \sim 1$ for $T_e \sim T \sim 100$ K, we may assume that electron heating occurs when $E'_{\text{eff},e}$ exceeds $E_{\text{crit},e}$. Note that the right-hand side of Equation (22) depends on $\langle \epsilon_e \rangle$ through P_ℓ and $\beta_e \propto 1/\nu_{en}$.

2.5. An Example

Figure 1 illustrates how the kinetics of plasma particles depends on the relative orientation between \mathbf{E}' and \mathbf{B} . Here, we plot the mean energies and Hall parameters of electrons and ions as a function of E' for two extreme cases of $\mathbf{E}' \parallel \mathbf{B}$ and $\mathbf{E}' \perp \mathbf{B}$. The parameters are chosen to be $T = 300$ K, $n_n = 10^{14} \text{ cm}^{-3}$, and $B = 1$ G. The values of T and n_n are close to those of the optically thin minimum-mass solar nebula model of Hayashi (1981) as measured at Earth's orbit. The value of B has been chosen so that the plasma beta $\beta_{\text{plasma}} \equiv 8\pi m_n n_n c_s^2 / B^2$, the ratio of the gas pressure to the magnetic pressure, is set to be ≈ 100 . For these parameters, one has $\beta_i \approx 0.03 \ll 1$ (see the bottom panel of Figure 1), and hence $\langle \epsilon_i \rangle$ is independent of the orientation of \mathbf{E}' . In contrast, the electron mean energy does depend on the orientation of \mathbf{E} because $|\beta_e| \approx 1\text{--}10$ as long as $E' \lesssim 10 \text{ V m}^{-1}$. In the particular case of $\mathbf{E}' \perp \mathbf{B}$, the approximation $E'_{\text{eff},e} \approx E' / |\beta_e|$ holds (see the discussion below Equation (19)), and therefore heating the electron requires $E' > E_{\text{crit},e}$ ($\approx 10 E_{\text{crit},e}$ in the example shown here).

Since $|\beta_e| \propto \nu_{en}^{-1} \propto \langle \epsilon_e \rangle^{-1/2}$, $|\beta_e|$ decreases with increasing $\langle \epsilon_e \rangle$ as shown in the bottom panel of Figure 1. This implies that the effects of magnetic fields on the electron conductivity becomes weaker as the electric fields heat electrons. We will come back to this point in Section 3.

3. CURRENTS IN A STRONG ELECTRIC FIELD: ANALYTIC ESTIMATES

Assuming that the relaxation timescales of plasma motions and charge reactions are short compared to the dynamical timescale of the neutral gas, the electric current flowing in the gas is approximately determined by the electric field in the neutral-comoving frame, the relation known as Ohm's law. Ohm's law specifies how strong electric field is needed to sustain an electric current of a given strength. In Paper

² Equation (22) is identical to Equation (17) of Mori & Okuzumi (2016) except that the factor $2/3$ in the previous expression has now been replaced by $9\pi P_\ell/64$. The new expression is more accurate because it takes into account inelastic energy losses, and because it uses the exact expression for ν_{en} (Equation (13)) whereas the previous expression used an approximate expression $\nu_{en} = n_n \sigma_{en} (v_e^2)^{1/2}$.

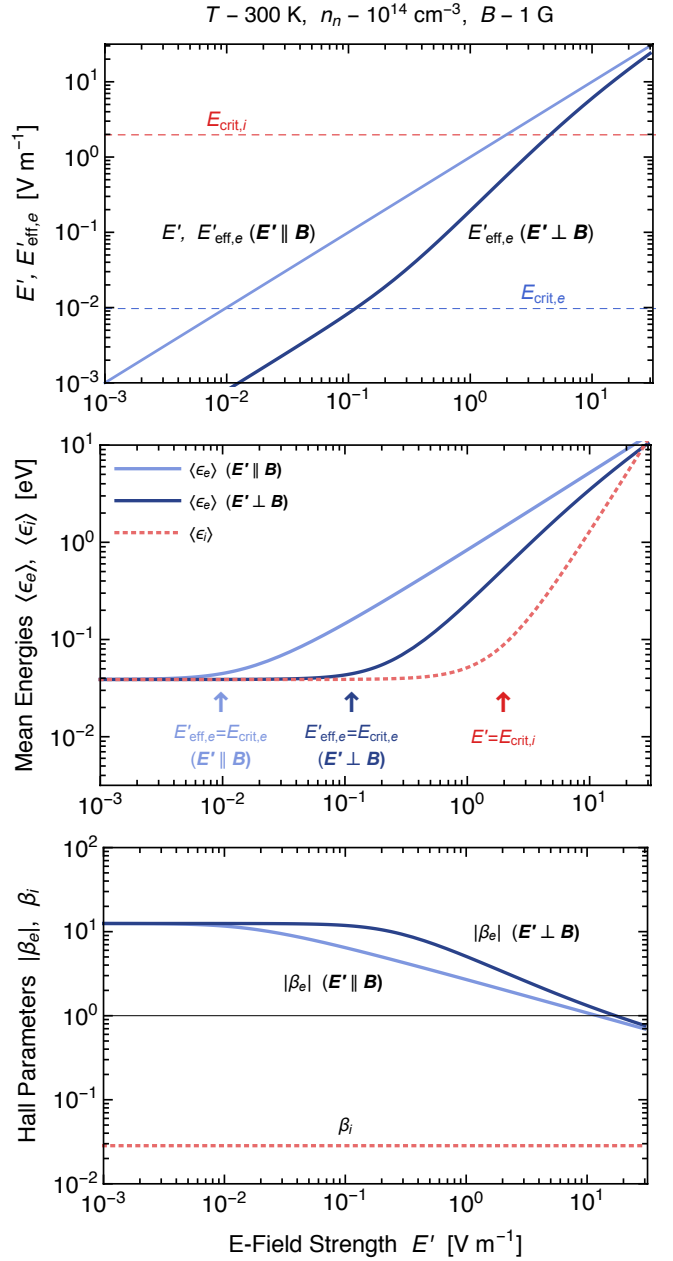


Figure 1. Effective electric field strengths, mean energies, and Hall parameters as a function of the electric field strength E' for $T = 300$ K, $n_n = 10^{14} \text{ cm}^{-3}$, and $B = 1$ G. Top panel: $E'_{\text{eff},e}$ for $\mathbf{E}' \parallel \mathbf{B}$ (solid black line) and for $\mathbf{E}' \perp \mathbf{B}$ (solid blue line), compared with the critical field strength for electron heating, $E'_{\text{eff},e}$ (dashed blue line). Note that $E'_{\text{eff},e} = E'$ for $\mathbf{E}' \parallel \mathbf{B}$, and that $E'_{\text{eff},e} \approx E'$ when $\beta_i \ll 1$ as considered here (see the bottom panel). Middle panel: $\langle \epsilon_e \rangle$ for $\mathbf{E}' \parallel \mathbf{B}$ (dark blue line) and for $\mathbf{E}' \perp \mathbf{B}$ (light blue line), and $\langle \epsilon_i \rangle$ (red dashed line). The light and dark blue arrows indicate $E'_{\text{eff},e} = E_{\text{crit},e}$, and the red arrow $E' = E_{\text{crit},i}$. Bottom panel: $|\beta_e|$ for $\mathbf{E}' \parallel \mathbf{B}$ (dark blue line) and for $\mathbf{E}' \perp \mathbf{B}$ (light blue line), and β_i (red dashed line).

I, we showed that in dusty environments like protoplanetary disks, there are upper limits on the electric current density

that can be realized without electrical breakdown. However, the derivation was limited to the case where the effect of magnetic field on the kinetic of plasmas is negligible, i.e., $|\beta_\alpha| \ll 1$. The aim of this section is to show that the same upper limits apply to the magnitude of the electric current density even in the presence of magnetic fields.

3.1. Generalized Ohm's Law

For given $\langle v_\alpha \rangle$ and n_α , the electric current density can be written as

$$\mathbf{J} = \sum_\alpha \mathbf{J}_\alpha, \quad \mathbf{J}_\alpha = q_\alpha n_\alpha \langle \mathbf{v}_\alpha \rangle. \quad (24)$$

When a magnetic field is present, $\langle \mathbf{v}_\alpha \rangle$ and hence \mathbf{J}_α are no longer parallel to \mathbf{E}' because of the magnetic Lorentz force (e.g., Nakano & Umebayashi 1986; Wardle & Ng 1999). It follows from Equation (16) that \mathbf{J}_α has a general form, often called the generalized Ohm's law,

$$\mathbf{J}_\alpha = \sigma_{O,\alpha} \mathbf{E}'_\parallel + \sigma_{H,\alpha} \hat{\mathbf{B}} \times \mathbf{E}'_\perp + \sigma_{P,\alpha} \mathbf{E}'_\perp, \quad (25)$$

where the coefficients

$$\sigma_{O,\alpha} = \frac{q_\alpha^2 n_\alpha}{\mu_{an} \nu_{an}}, \quad \sigma_{H,\alpha} = -\frac{\beta_\alpha \sigma_{O,\alpha}}{1 + \beta_\alpha^2}, \quad \sigma_{P,\alpha} = \frac{\sigma_{O,\alpha}}{1 + \beta_\alpha^2} \quad (26)$$

represent the contributions of charge species α to the Ohmic, Hall, and Pedersen conductivities, respectively. The generalized Ohm's law reduces to the standard Ohm's law $\mathbf{J}_\alpha = \sigma_{O,\alpha} \mathbf{E}'$ in the limit of $|\beta_\alpha| \rightarrow 0$.

The expression of the generalized Ohm's law in the vector form is much more complex than that of the standard Ohm's law. However, one can show from Equation (25) that the magnitude of the current, $J_\alpha \equiv |\mathbf{J}_\alpha|$, has a much simpler expression

$$J_\alpha = \sigma_{O,\alpha} E'_{\text{eff},\alpha}, \quad (27)$$

where $E'_{\text{eff},\alpha}$ is the effective electric field strength already introduced in Equation (19). Equation (27) is formally identical to the scalar version of the standard Ohm's law, $J_\alpha = \sigma_{O,\alpha} E'$, except that E' has now been replaced by $E'_{\text{eff},\alpha}$. As discussed in Section 2, ν_{an} for ions is constant, and that for electrons depends on \mathbf{B} and \mathbf{E}' only through $E'_{\text{eff},e}$. Therefore, if n_α depends only on $E'_{\text{eff},\alpha}$, so does J_α , and the dependence is identical to that of J_α on E' for vanishing magnetic field.

3.2. Upper limits on the Currents in a Dusty Gas

Protoplanetary disks are weakly ionized plasmas with an typical ionization fraction much below 10^{-10} in their inner part. They are also dusty plasmas where small dust grains affect the plasma densities and can even contribute to the overall charge neutrality of the dust–gas mixture (e.g., Sano et al. 2000; Ilgner & Nelson 2006; Wardle 2007; Bai & Goodman 2009; Okuzumi 2009). As highlighted in Paper I, plasma

heating accelerates the adsorption of the plasma particles onto small dust grains, thus suppressing the electric currents in the mixture. We here show that the same happens even in the presence of magnetic fields.

When small dust grains are so abundant that electron capture by the grains outpaces electron–ion recombination in the gas, n_e is approximately given by (Equation (58) of Paper I)

$$n_e \approx \frac{\zeta n_n}{\pi a^2 n_d \langle v_e \rangle C_e}, \quad (28)$$

where ζ is the ionization rate of the neutral gas, a and n_d are the size and number density of the grains, and C_e is a dimensionless factor typically in the range 0.01–1. In Equation (28), the factor $\pi a^2 n_d \langle v_e \rangle$ corresponds to the rate of electron capture for neutral grains, while C_e expresses how much the electron–grains collisions are suppressed when the grains are negatively charged (see Equation (B3) for its expression under the Maxwellian approximation). Since $\langle v_e \rangle \propto \langle \epsilon_e \rangle^{1/2}$ (see Equation (9)), n_e decreases with increasing $E'_{\text{eff},e}$ at $E'_{\text{eff},e} > E_{\text{crit},e}$.

When Equation (28) holds, the magnitude of the electron current has a useful limiting expression in the strong field limit $E' \gg E_{\text{crit},e}$. Substitution of Equation (28) together with Equations (9) and (13) into $J_e = \sigma_{O,e} E'_{\text{eff},e}$ gives

$$J_e \approx \frac{\zeta e^2}{\pi a^2 n_d C_e} \frac{9\pi E'_{\text{eff},e}}{64\sigma_{en} \langle \epsilon_e \rangle}. \quad (29)$$

For $E'_{\text{eff},e} \gg E_{\text{crit},e}$, Equation (22) has a limiting expression

$$\langle \epsilon_e \rangle \approx \frac{3}{16} \sqrt{\frac{3\pi P_\ell m_n}{2m_e}} \frac{e E'_{\text{eff},e}}{n_n \sigma_{en}}, \quad (30)$$

and hence we obtain $J_e \approx J_{e,\text{max}}$, where

$$J_{e,\text{max}} \equiv \frac{1}{C_e} \sqrt{\frac{3\pi m_e}{8P_\ell m_n}} \frac{\zeta e n_n}{\pi a^2 n_d}. \quad (31)$$

Equation (31) is almost identical to Equation (60) of Paper I, but the new expression accounts for the inelastic energy losses in electron–neutral collisions.

The most important property of $J_{e,\text{max}}$ is that it does not depend on the electric field strength except through C_e and P_ℓ . Ignoring the dependence of C_e and P_ℓ on $E'_{\text{eff},e}$, the electron conductivity $\sigma_{O,e}$ is inversely proportional to $E'_{\text{eff},e}$, because both n_e and ν_{en}^{-1} scale as $\langle v_e \rangle^{-1} \propto (E'_{\text{eff},e})^{-1/2}$. This cancels the linear dependence of $J_e = \sigma_{O,e} E'_{\text{eff},e}$ on $E'_{\text{eff},e}$. In fact, $J_{e,\text{max}}$ increases or decreases slowly with $E'_{\text{eff},e}$ depending on the behavior of P_ℓ and C_e as we demonstrate in Section 3.

Similarly, the limiting value of the ion current J_i at $E'_{\text{eff},i} \gg E_{\text{crit},i}$ is given by (Johansen & Okuzumi 2018)

$$J_{i,\text{max}} = \frac{1}{C_i} \frac{\zeta e n_n}{\pi a^2 n_d}, \quad (32)$$

where C_i expresses the enhancement of the ion–grain collision frequency due to their Coulomb attraction (see Equations (B5) and (B6) for its expression under the Maxwellian approximation). As we demonstrate in Section 4, J_i dominates the total current only when negatively charged small grains are so abundant that the electrons in the gas gets depleted compared to the ions in the gas. In that case, it is usually safe to assume $C_i \approx 1$ (Paper I; Johansen & Okuzumi 2018).

If we rewrite n_n/n_d in terms of the dust-gas mass ratio $f_{\text{dg}} \equiv m_d n_d / (m_n n_n)$, where $m_d = 4\pi\rho_{\text{int}}a^3/3$ and ρ_{int} are the mass and internal density of the grains, respectively, we obtain

$$J_{e,\text{max}} \approx 1.4 \times 10^{-8} \left(\frac{0.02}{C_e} \right) \left(\frac{1}{P_\ell} \right)^{1/2} \left(\frac{10^{-6}}{f_{\text{dg}}} \right) \left(\frac{\rho_{\text{int}}}{3 \text{ g cm}^{-3}} \right) \left(\frac{a}{0.1 \mu\text{m}} \right) \times \left(\frac{\zeta}{10^{-18} \text{ s}^{-1}} \right) \text{ A m}^{-2}, \quad (33)$$

$$J_{i,\text{max}} \approx 1.6 \times 10^{-8} \left(\frac{1}{C_i} \right) \left(\frac{10^{-6}}{f_{\text{dg}}} \right) \left(\frac{\rho_{\text{int}}}{3 \text{ g cm}^{-3}} \right) \left(\frac{a}{0.1 \mu\text{m}} \right) \times \left(\frac{\zeta}{10^{-18} \text{ s}^{-1}} \right) \text{ A m}^{-2}. \quad (34)$$

4. CURRENTS IN A STRONG ELECTRIC FIELD: CALCULATIONS WITH AN IONIZATION MODEL

We here demonstrate that the magnitude of the current density in a dusty gas indeed plateaus out at high electric field strengths. To do that, we compute n_α as a function of the electric field strength consistently with the velocity distribution of plasma particles. We also study how the electric conductivities and magnetic resistivities (to be introduced in Section 4.3) depend on the electric field strength.

4.1. Ionization Model

We employ a simplified charge reaction model developed in Paper I. In this model, we only consider one species of positive ions and one species of charged dust grains. The grains are assumed to have a narrow charge distribution peaked at the mean charge Ze , and the dispersion of the grain charge is neglected. The charge reactions we consider are the ionization by external ionizing sources, recombination of the electrons and ions in the gas, and adsorption of the plasma particles to the grains.

Under these assumptions, the rate equations for the ion and electron number densities n_i and n_e are given by

$$\frac{dn_i}{dt} = \zeta n_n - K_{\text{rec}} n_i n_e - K_{di} n_d n_i, \quad (35)$$

$$\frac{dn_e}{dt} = \zeta n_n - K_{\text{rec}} n_i n_e - K_{de} n_d n_e, \quad (36)$$

respectively, where ζ is the rate of external ionization, and $K_{d\alpha}$ ($\alpha = i, e$) and K_{rec} are the rate coefficients for gas-phase

recombination and plasma adsorption onto the grains, respectively. The dimensionless numbers C_e and C_i appearing in Equations (31) and (34) are related to K_{de} and K_{di} as $C_e = K_{de}/(\pi a^2 \langle v_e \rangle)$ and $C_i = K_{di}/(\pi a^2 \langle v_i \rangle)$, respectively, where $\langle v_i \rangle$ is the mean speed of the ions (see Appendix B). The reaction rate coefficients depend on the velocity distribution of ions and electrons, and we use the expressions under the offset Maxwell approximation given in Appendix B. The adsorption rate coefficients depend on the grain charge Z , which is related to n_i and n_e via the charge neutrality of the gas–dust mixture,

$$n_i - n_e + Zn_d = 0. \quad (37)$$

We assume steady state $dn_i/dt = dn_e/dt = 0$ and solve Equations (35)–(37) for n_i , n_e , and Z under the steady state conditions as a function of E' and the relative orientation between \mathbf{E}' and \mathbf{B} (below assumed to be either parallel or perpendicular to each other). The solution of the equations is searched for using the semianalytic approach detailed in Section 3.2.4 of Paper I. The solution generally satisfies $Z < 0$.

The adopted model neglects the ionization of the neutral gas by electrically heated electrons. In Paper I, we showed that this impact ionization dominates over external ionization when $\langle \epsilon_e \rangle \gtrsim 3 \text{ eV}$, for which the number of electrons with a kinetic energy above the H_2 ionization potential of 15.4 eV is substantial. When the electric field is strong enough to fulfill this condition, the impact ionization causes electrical breakdown, leading to an abrupt increase in the electric current similar to lightning. However, we found in Paper I that this lightning-like current is unstable to perturbations when the charged grains are the dominant negative charge carriers. Because the stability issue of the lightning-like discharge is not the focus of this paper, we simply neglect impact ionization and instead restrict the electric-field strength to below the threshold corresponding to $\langle \epsilon_e \rangle = 3 \text{ eV}$. Note that it is safe to use our approximate expression for P_ℓ (Equation (15)) below this threshold.

4.2. Parameter Choice

As in Section 2.5, we consider the inner part of protoplanetary disks and adopt $T = 300 \text{ K}$ and $n_n = 10^{14} \text{ cm}^{-3}$. The ionization rate ζ is taken to be $\zeta = 10^{-18} \text{ s}^{-1}$ assuming that the gas is mainly ionized by short-lived radionuclides (for which $\zeta \sim 10^{-20}$ – 10^{-18} s^{-1} ; see Umebayashi & Nakano 1981, 2009; Stepinski 1992; Cleaves et al. 2013). This is a reasonable assumption for the dense part of disks where external ionizing sources such as cosmic rays and X-rays are greatly attenuated. Dust grains are assumed to have a radius of $a = 0.1 \mu\text{m}$.

We consider two cases of $f_{\text{dg}} = 10^{-6}$ and 10^{-4} (henceforth cases 1 and 2, respectively). As discussed by Okuzumi (2009) and in Paper I, the ionization state of a gas–dust mixture depends on whether $n_e > |Z|n_d$ or $n_e < |Z|n_d$, i.e.,

whether the dominant negative charge carriers are the electrons in the gas or the negatively charged grains. We have selected the two values of f_{dg} so that the two extreme conditions $n_e \gg |Z|n_d$ and $n_e \ll |Z|n_d$ are realized in cases 1 and 2, respectively, in the limit of $E' \rightarrow 0$. If $n_e \gg |Z|n_d$, Equation (37) gives $n_i \approx n_e$, and one generally has $J_e \gg J_i$ because electrons are much more mobile than ions. In the opposite case of $|Z|n_d \gg n_e$, the number of electrons in the gas is typically two orders of magnitude smaller than that of ions in the gas, and for this reason J_i can be comparable to or even dominate over J_e . The Coulomb reduction factor C_e is determined by which regime applies, with $C_e \approx 0.02$ – 0.1 for $n_e \gg |Z|n_d$ and $C_e \approx 1$ for $n_e \ll |Z|n_d$ (see Figure 9 of Paper I).

4.3. Magnetic Resistivities

To quantify the non-ideal MHD effects, it is useful to introduce the magnetic resistivities for Ohmic diffusion, Hall drift, and ambipolar diffusion defined by (see, e.g., Wardle 2007)

$$\eta_O = \frac{c^2}{4\pi\sigma_O}, \quad (38)$$

$$\eta_H = \frac{c^2\sigma_H}{4\pi(\sigma_H^2 + \sigma_P^2)}, \quad (39)$$

$$\eta_A = \frac{c^2\sigma_P}{4\pi(\sigma_H^2 + \sigma_P^2)} - \eta_O, \quad (40)$$

respectively, where $\sigma_O = \sum_\alpha \sigma_{O,\alpha}$, $\sigma_H = \sum_\alpha \sigma_{H,\alpha}$, and $\sigma_P = \sum_\alpha \sigma_{P,\alpha}$ are the Ohmic, Hall, and Pedersen conductivities accounting for the contributions of all charged species. In general, the dominant non-ideal effect has the largest resistivity.

If $n_i \approx n_e$ as in case 1, the resistivities satisfy simple relations (Wardle 2007)

$$\eta_O \approx \frac{c^2}{4\pi\sigma_{O,e}}, \quad \eta_H \approx |\beta_e|\eta_O, \quad \eta_A \approx \beta_i\eta_H \approx \beta_i|\beta_e|\eta_O, \quad (41)$$

and therefore all the resistivities simply scale as $\sigma_{O,e}^{-1}$. Furthermore, if $\beta_i < 1 < |\beta_e|$, then η_H is larger than η_O and η_A , indicating that Hall drift dominates over Ohmic and ambipolar diffusion. If $n_i \gg n_e$ as in case 2, the dependences of η_H and η_A are generally complex (see, e.g., Xu & Bai 2016). In contrast, η_O is always inversely proportional to σ_O , and hence to the number densities of charged particles, no matter whether $n_i = n_e$ or not.

4.4. Results: Case 1

We begin by studying how plasma heating changes the charge reaction balance in this case. The top row of Figure 2 shows the number densities of ions and electrons in the gas, n_i and n_e , as well as the number density of electrons adsorbed

on grain surfaces, $-Zn_d$, as a function of E' for two extreme orientations of \mathbf{E}' relative to \mathbf{B} . As mentioned in Section 4.2, case 1 is designed so that the condition $n_i \approx n_e \gg |Z|n_d$ holds in the limit of small E' . As E' increases and the electric heating of electrons sets in ($E'_{\text{eff},e} = E_{\text{crit},e}$), $|Z|$ starts to increase because the heated electrons collide with and adsorb onto dust grains more frequently (Paper I). This also causes the decrease of n_e with increasing E' . In this particular example, the charged grains become the dominant negative charge carriers $|Z|n_d > n_e$ at $E' \gtrsim 1 \text{ V m}^{-1}$.

The second row of Figure 2 shows the magnitude of the total current density, J , as well as of the ion and electron current densities, J_i and J_e . As stated in Section 4.2, the electron current dominates in the case of $n_e \approx n_i$. The results shown here demonstrate that the total current for such a case approaches $J_{\text{max},e}$ given by Equation (31), irrespective of the orientation of \mathbf{E}' . It is important to note that the value of E' required to heat electrons does depend on its orientation, with the $\mathbf{E}' \perp \mathbf{B}$ case requiring 10 times higher E' than the $\mathbf{E}' \parallel \mathbf{B}$ case (see the blue arrows in the top panels of Figure 2 for the onset of electron heating). This illustrates that J should be viewed as a function of $E'_{\text{eff},e}$ rather than of E' as long as the electric heating of ions is negligible.

The bottom two rows of Figure 2 plot the conductivities and resistivities as a function of E' . Because $n_i \approx n_e$, the resistivities satisfy the relations given by Equation (41). In this particular case, one has $\beta_i < 1 < |\beta_e|$ (see Figure 1), and therefore η_H is the largest. Because $\sigma_{O,e}$ decreases with increasing E' ³, all resistivities increase with E' . Moreover, since $|\beta_e|$ is a decreasing function of E' (Figure 1), $\eta_H \approx |\beta_e|\eta_O$ increases more slowly than η_O , and hence the difference between the two resistivities decrease toward higher E' .

4.5. Results: Case 2

Case 2 serves as an example where the condition $n_i \approx |Z|n_d \gg n_e$ holds (top row of Figure 3). At $E'_{\text{eff},e} > E_{\text{crit},e}$, n_e decreases with increasing E' for the reason described in Section . For the same reason, n_i also decreases at $E'_{\text{eff},i} > E_{\text{crit},i}$.

Because $n_i \gg n_e$ in case 2, J_i gives a relatively large contribution to J as shown in the second row of Figure 3. For $\mathbf{E}' \parallel \mathbf{B}$, J_i dominates over J_e as the latter plateaus out at $J_{e,\text{max}}$. At $E' > E_{\text{crit},i}$, n_i also decreases with E' , and consequently J_i relaxes into a constant $J_{i,\text{max}}$ given by Equation (34) as predicted in Section 3.2.

The bottom two rows of Figure 3 show the conductivities and resistivities versus E' for case 2. As in case 1, the conductivities decrease monotonically with increasing E' , and hence η_O ($\propto \sigma_O^{-1}$) increases with E' . In contrast, η_A and η_H

³ This follows from $\sigma_{O,e} \propto (C_e P_\ell^{1/2} E'_{\text{eff},e})^{-1}$, $P_\ell \propto \langle \epsilon_e \rangle^{-1/2} \propto (E'_{\text{eff},e})^{-1/2}$, and C_e being an increasing function of $E'_{\text{eff},e}$.

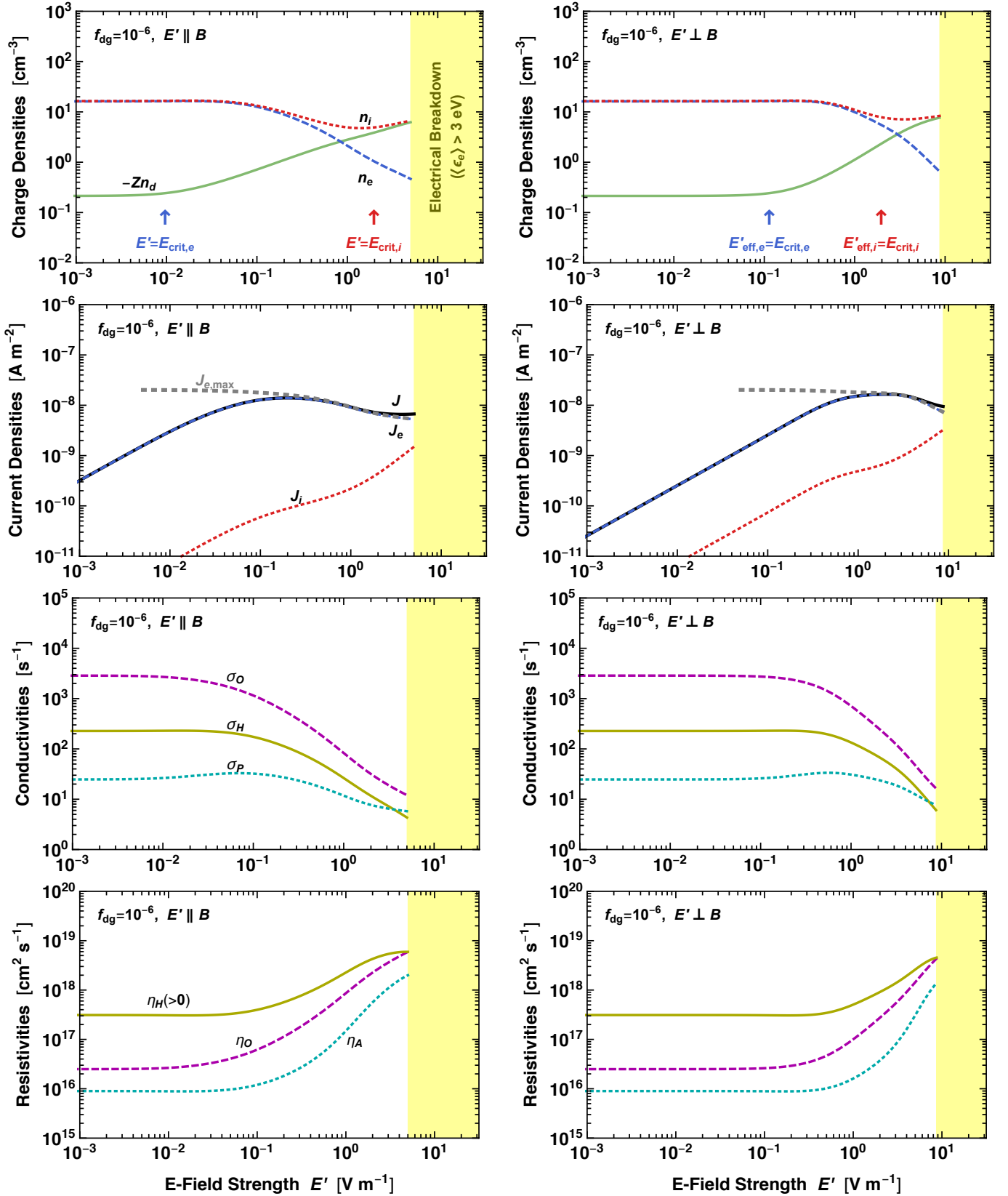


Figure 2. Number densities of charges in the gas phase and on dust grains (top row), electric currents (second row), electric conductivities (third row), and magnetic diffusivities (bottom row) as a function of the electric field strength E' for case 1 ($f_{dg} = 10^{-6}$). The left and right columns are for electric field parallel and perpendicular to the magnetic field, respectively. The yellow shaded area marks the field range where $\langle \epsilon_e \rangle > 3$ eV, at which electrical breakdown of the gas occurs due to impact ionization by hot electrons (see Paper I). The blue and red arrows in the top row indicate $E'_{\text{eff},e} = E_{\text{crit},e}$ and $E'_{\text{eff},i} = E_{\text{crit},i}$, respectively. The thick dashed lines in the second row show the maximum electron current $J_{\text{max},e}$ given by Equation (31), with C_e given by Equation (B3). Because $J \approx J_e$ in these particular examples, the lines for J and J_e in the second row overlap.

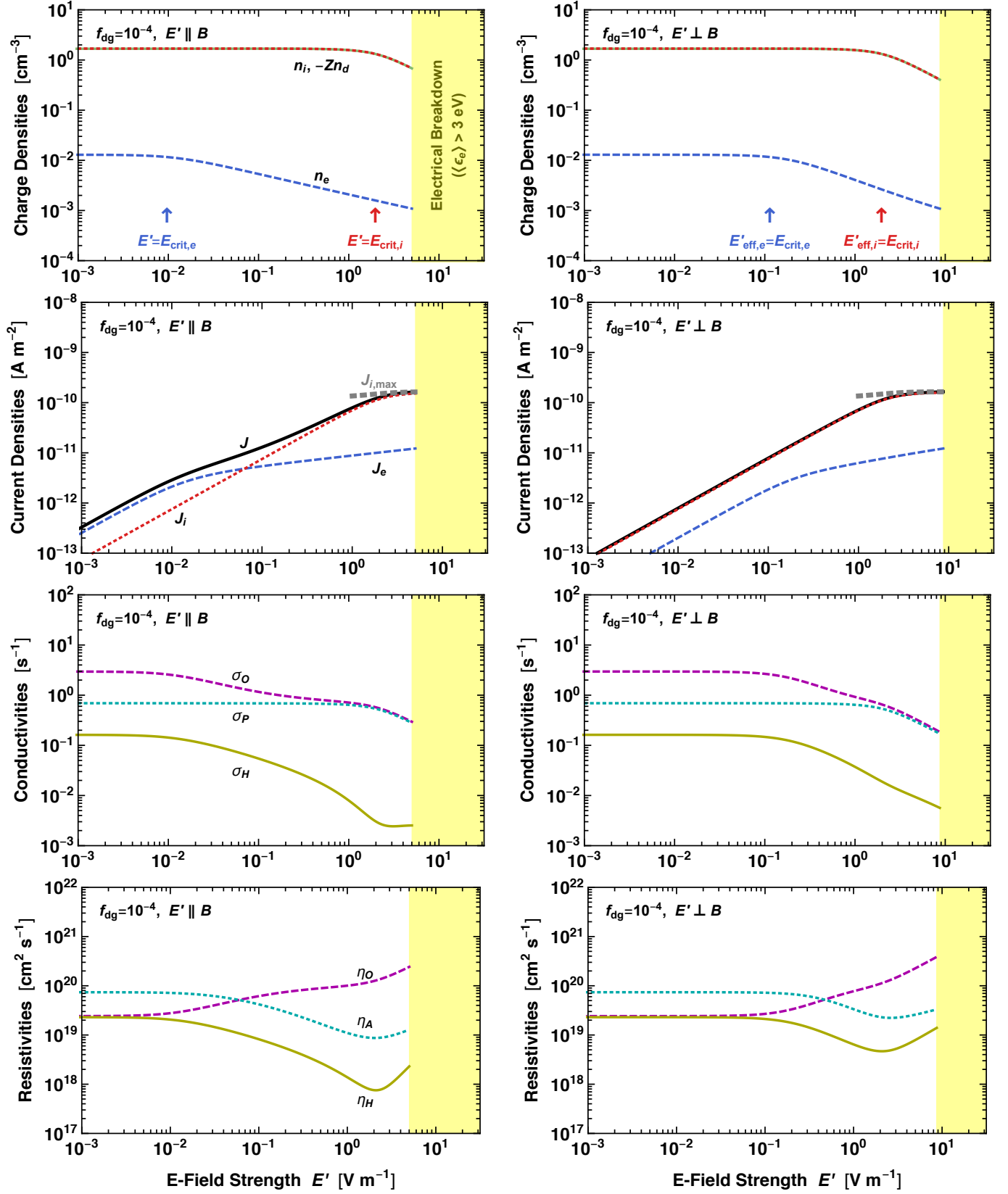


Figure 3. Same as Figure 2, but for case 2 ($f_{dg} = 10^{-4}$). The thick dashed lines in the second row indicate the maximum ion current $J_{i,max}$ given by Equation (34), with C_i given by Equation (B5).

decrease until E' reaches $E_{\text{crit},i}$, contrary to case 1. As a consequence, η_O dominates over η_A at $E' \gtrsim 10E_{\text{crit},e}$.

The reason why η_A and η_H decrease with E' is the following. In case 2, electrons are so depleted from the gas phase that $\sigma_P \approx \sigma_{P,i}$. In contrast, σ_H is still dominated by $\sigma_{H,e}$, and is smaller than σ_P as shown in the third row of Figure 3. From these relations, we obtain $\eta_H \propto \sigma_{H,e}/\sigma_{P,i}^2$ and $\eta_A \propto 1/\sigma_{P,i} - 1/\sigma_O$. At $E' < E_{\text{crit},i}$, $\sigma_{P,i} (\propto n_i)$ is constant, and therefore $\eta_H \propto \sigma_{H,e}$ is a decreasing function of E' . In addition, at $E' \gtrsim 10E_{\text{crit},e}$, the electrons in the gas are further depleted so that σ_O approaches $\sigma_{O,i}$. However, because $\beta_i \ll 1$ in this example (see Equation (26)), $\sigma_{O,i}$ is approximately equal to $\approx \sigma_{P,i}$. Therefore, $\eta_A \propto 1/\sigma_{P,i} - 1/\sigma_O$ vanishes as σ_O approaches $\sigma_{O,i}$.

As is obvious from the above analytic argument, how η_H and η_A behave as a function of E' depends on the values of β_i and β_e as well as on n_e/n_i . Exploring these dependences over a wide parameter space will be interesting future work, but is not the subject of this paper. It is perhaps more important to emphasize that the Ohmic resistivity η_O never decreases with E' , and that it tends to dominate over the other two resistivities at sufficiently large E' . The second point is a natural consequence of the general property that Ohmic diffusion dominates when $|\beta_e|$ falls below 1 (Xu & Bai 2016). Electron heating causes a decrease in $|\beta_e|$, and hence tends to make Ohmic diffusion the dominant nonideal MHD effect.

5. IMPLICATIONS FOR MHD IN PROTOPLANETARY DISKS

The most important finding of this study is that plasma heating places upper limits on the electric currents even when magnetic fields strongly affect the plasma motions, corresponding to the case where Hall drift or ambipolar diffusion dominates over Ohmic diffusion. Any MHD motion that can produce a current larger the limits would either cause electrical breakdown of the gas (Inutsuka & Sano 2005; Muranushi et al. 2012) or would get suppressed before the breakdown sets in (Mori et al. 2017). The upper limits decrease with increasing the abundance of small dust grains. Moreover, it is shown by (Paper I) that if the grains are the dominant negative charge carriers, the breakdown current is unstable to perturbations. Therefore, we can speculate that any MHD motion that produces a current exceeding the limits would be stably sustained only if small grains are heavily depleted.

The next question is then whether the MHD motions of real protoplanetary disks would indeed produce such a high electric current. In Paper I and Mori & Okuzumi (2016), we pointed out that the small-scale currents produced by fully developed MRI turbulence can indeed exceed the limits. However, as mentioned in Section 1, recent studies show that MRI-driven turbulence is unlikely to operate in most part of the disks if all three non-ideal MHD effects are taken into

account. Based on the current understanding of the MHD in protoplanetary disks, we here consider more coherent gas motions on a larger scale. A candidate that drives such a motion is the HSI, which has recently been found to generate a large-scale magnetic field (Kunz & Lesur 2013; Bai 2014, 2017; Lesur et al. 2014). The MHD simulations by Bai (2015, 2017) show that a large-scale field produced by the HSI is in some cases accompanied by a strong current layer near the midplane (see Section 5.1 of Bai 2015; Section 5.2 of Bai 2017). Because the strong magnetic fields generated by the HSI can provide a high level of accretion stress, it is important to assess whether the upper limits on the electric current could affect the saturation level of the HSI. We note that a strong current can also occur on the disk surface where the ionization rate is higher than in the midplane (e.g., Bai & Stone 2013b; Gressel et al. 2015), but such a current is less likely to be relevant because the upper limits increase with ionization rate (see Equation (31) and (34)).

To estimate the magnitude of the current associated with such a large-scale gas motion, we make use of Ampere's law

$$\mathbf{J} = \frac{c}{4\pi} \nabla \times \mathbf{B}. \quad (42)$$

We assume that the magnetic field produced by the HSI has typical magnitude \bar{B} and length scale L over which the magnetic field lines are bent. Using Equation (42), one can estimate that the electric current that produces the magnetic field has a typical current density of $\bar{J} \sim c\bar{B}/(4\pi L)$. We rewrite this as

$$\begin{aligned} \bar{J} &\sim \sqrt{\frac{\rho}{2\pi\beta_{\text{pl}}}} \frac{c\Omega H}{L} \\ &\sim 10^{-8} \left(\frac{H}{L}\right) \left(\frac{\rho}{10^{-9} \text{ g cm}^{-3}}\right)^{1/2} \left(\frac{100}{\beta_{\text{pl}}}\right)^{1/2} \left(\frac{\Omega}{2\pi \text{ yr}^{-1}}\right) \text{ A m}^{-2}, \end{aligned} \quad (43)$$

where $\beta_{\text{pl}} = 8\pi\rho c_s^2/\bar{B}^2$ is the plasma beta and $H = c_s/\Omega$ is the gas scale height, with ρ , c_s , and Ω being the mass density, sound speed, and local orbital frequency of the disk gas, respectively. In the case of the HSI, the induced magnetic field near the midplane has $\beta_{\text{pl}} \sim 100$ and $L \sim H$ (see Figure 8 of Bai 2017).

Now we compare \bar{J} given by Equation (43) with the upper limits $J_{e,\text{max}}$ and $J_{i,\text{max}}$ given by Equations (31) and (34). As an example, we consider the minimum-mass solar nebula model (Weidenschilling 1977; Hayashi 1981), in which $\rho \sim 10^{-9}(r/1 \text{ au})^{-11/4} \text{ g cm}^{-3}$ at the midplane and $\Omega = 2\pi(r/1 \text{ au})^{-3/2} \text{ yr}^{-1}$, with r being the distance from the central star (assumed to be of one solar mass). As in Section 4, we take $\zeta \sim 10^{-18} \text{ s}^{-1}$ and $a_0 \sim 0.1 \mu\text{m}$, and parametrize the amount of small dust grains that contributes charge reactions with the dust-to-gas mass ratio f_{dg} . For $\beta_{\text{pl}} \sim 100$ and $L \sim H$, one finds that \bar{J} exceeds the limits at $r \lesssim 1 \text{ au}$ and 3 au if $f_{\text{dg}} \sim 10^{-6}$ and 10^{-4} , respectively.

To summarize, we have found that the upper limits on the electric current imposed by plasma heating can indeed affect large-scale MHD motions in the inner ~ 1 au of protoplanetary disks. This could potentially have a substantial influence on the accretion of the inner disk regions. If such a motion can recurrently trigger electrical breakdown near the midplane, this could also potentially lead to the formation of chondrules through flash heating in the lightning current (e.g., Whipple 1966; Desch & Cuzzi 2000). However, it is also possible that the enhanced Ohmic resistivity at $E' > E_{\text{crit},e}$ diffuses the midplane current layer before the electric field strength reaches the breakdown threshold. If this is the case, the upper limits on the electric current would rather act to push the midplane current layer toward one side of the disk surface, as often observed in MHD simulations that assume a high magnetic diffusivity near the midplane (e.g., Bai & Stone 2013b; Lesur et al. 2014; Béthune et al. 2017; Mori et al. 2019). Self-consistent simulations including both nonideal MHD and plasma heating by electric fields are needed to investigate whether recurrent discharge or the escape of the current layer from the disk midplane is a more realistic outcome.

Even if the electric field induced by gas motions is not strong enough to directly cause electrical breakdown, the limits on the currents can help breakdown via charge separation by positron emission from dust particles (Johansen & Okuzumi 2018) and other potential mechanisms. This possibility should also be examined in future MHD simulations including all non-ideal MHD effects and plasma heating. Finally, we note that the HSI is absent when the disk's vertical magnetic field is anti-aligned with the rotation axis. In such a disk, Hall drift acts to weaken the magnetic field, and therefore the effects of plasma heating on disk accretion would be less important.

6. SUMMARY

Following Paper I, we have studied how plasma heating by strong electric fields affects the electric current in dusty protoplanetary disks. The new formulation presented in this paper fully takes into account the effects of magnetic fields on the motion of plasma particles, thus allowing us to treat Hall drift and ambipolar diffusion in addition to Ohmic diffusion. We have also included the energy losses of electrons through inelastic collisions with neutrals, which were also neglected in our previous work. Our key findings are summarized as follows.

1. In the presence of both electric and magnetic fields, the temperature of a charged species (ions or electrons) is determined by its effective electric field strength

(Equation (19); see also Golant et al. 1980). Substantial heating of a charged species occurs when its effective field strength exceeds the critical field strength, which is also species-dependent (Equations (21) and (23)).

2. The upper limits on the ion and electron currents discovered in Paper I for the spacial case of zero magnetic field hold even with a magnetic field (Equations (31) and (34)). Any electric current exceeding the limits is only realized with electrical breakdown of the gas.
3. A large-scale electric current produced by an MHD motion in the inner part of protoplanetary disks can exceed the upper limits (Section 5). A potential mechanism that can drive such a motion near the midplane is the HSI, which operates when the vertical magnetic flux is aligned with the direction of the disk rotation axis. Based on our previous MHD simulations (Muranushi et al. 2012; Mori et al. 2017), we predict that a strong current layer near the midplane could either trigger recurrent electrical breakdown or get suppressed by the increasing ohmic diffusion with increasing electric field strength. The former outcome could lead to chondrule formation (e.g., Whipple 1966; Desch & Cuzzi 2000; Johansen & Okuzumi 2018) and the latter outcome could result in migration of a strong current layer to one side of the disk surface (e.g., Bai & Stone 2013b; Lesur et al. 2014; Béthune et al. 2017; Mori et al. 2019). Self-consistent MHD simulations including all non-ideal effects and plasma heating are needed to investigate which outcome occurs in realistic conditions.
4. Inelastic collisions between electrons and neutrals suppress the electron energy, but only by a factor of $\lesssim 4$ as long as the electrons are not hot enough to cause gas ionization (Appendix A). The inelastic energy losses have little effect on the onset of electron heating.

We are grateful to Xuening Bai for providing us with the data of his MHD simulations (Bai 2015, 2017), which motivated us to derive an analytic estimate of the current density presented in Section 5. We also thank the anonymous reviewer for comments that helped improve the manuscript. This work was supported by JSPS KAKENHI Grant Numbers JP16H04081, JP16K17661, JP17K18812, JP18H05438, and JP19K03926.

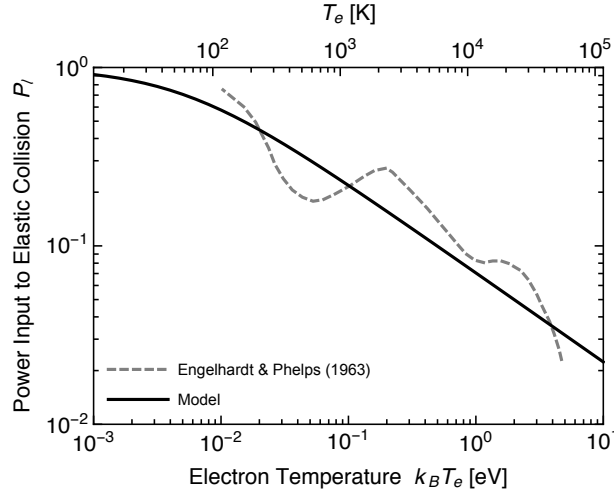


Figure 4. Fractional power input to elastic collision, P_ℓ , as a function of the electron temperature T_e . The dashed curve shows the theoretical estimate by Engelhardt & Phelps (1963) based on experiments (see their Figure 15), while the solid curve shows our analytic fit (Equation (15)).

APPENDIX

A. A SIMPLE MODEL FOR P_ℓ

We here derive a simple analytic expression for P_ℓ , the fractional contribution of elastic collisions to the electron energy losses through collisions with neutrals, based on the theoretical calculation by Engelhardt & Phelps (1963). They derived the fractional power inputs to the elastic and inelastic energy losses in H_2 gas based on electron swarm experiments. The inelastic losses include the rotational, vibrational, and electronic excitation losses and the ionization loss. The dashed curve in Figure 4 shows P_ℓ versus the electron temperature T_e taken from Figure 15 of Engelhardt & Phelps (1963).⁴ Overall, P_ℓ decreases from ≈ 1 to ~ 0.02 as T_e goes from 10^{-2} eV to 10 eV. The dips in P_ℓ at $T_e \sim 0.05$ eV, 0.1 eV, and 5 eV correspond to the energy losses due to the rotational, vibrational, and electronic excitation of H_2 , respectively. The contribution of the ionization loss is less significant than that of electronic excitation loss as long as $T_e \lesssim 10$ eV (see Figure 15 of Engelhardt & Phelps 1963). We find that the overall trend can be approximated by a simple function

$$P_\ell = \left(1 + \frac{k_B T_e}{0.005 \text{ eV}}\right)^{-1/2}, \quad (\text{A1})$$

which is shown by the solid curve in Figure 4. Equation (A1) reproduces the result of Engelhardt & Phelps (1963) to within a factor of 2. We note that our analytic fit could overestimate P_ℓ at $T_e > 4$ eV, where we expect larger energy losses due to electronic excitation and ionization. In fact, Figure 15 of Engelhardt & Phelps 1963 indicates that these energy losses quickly increase at $T_e > 2$ eV. Substitution of $k_B T_e = (2/3)\langle\epsilon_e\rangle$ into Equation (A1) gives Equation (15) in the main text.

To illustrate how much the inelastic energy losses affect electron heating, we compare in Figure 5 the mean electron energy $\langle\epsilon_e\rangle$ (Equation (18)) for P_ℓ given by Equation (15) with $\langle\epsilon_e\rangle$ for purely elastic collisions, $P_\ell = 1$, as a function of E' . Here we take $T = 300$ K and $n_n = 10^{14} \text{ cm}^{-3}$ as in Figure 1. Since $P_\ell \sim 1$ at $T_e \approx T \sim 100$ K, inelastic losses have little effect on the onset of electron heating. At $E > E_{\text{crit},e}$, the electron energy scales as $\langle\epsilon_e\rangle \propto E'^{4/5}$, which directly follows from the high-field expressions of Equations (15) and (22), $P_\ell \propto T_e^{-1/2} \propto \langle\epsilon_e\rangle^{-1/2}$ and $\langle\epsilon_e\rangle \propto P_\ell^{1/2} E'$. For example, at $E' = 5 \text{ V m}^{-1}$, we obtain $\langle\epsilon_e\rangle \approx 3$ eV with inelastic energy losses, which is about four times lower than $\langle\epsilon_e\rangle$ with no inelastic losses. Therefore, as long as the electron energy is not high enough to cause electrical breakdown (≈ 3 eV), the inelastic energy losses only cause a suppression of the electron mean energy by a factor of $\lesssim 4$.

B. REACTION RATE COEFFICIENTS

The derivation of the adsorption rate coefficients K_{de} and K_{di} under the Maxwellian approximation can be found in the literature Shukla & Mamun (e.g., 2002), so we here only show the results. The adsorption rate coefficient for electrons with the velocity

⁴ Engelhardt & Phelps (1963) express P_ℓ as a function of the “characteristic energy” $\epsilon_K = eD/\mu$, where D and μ are the diffusion coefficient and electrical mobility of electrons. We here assume Maxwellian plasmas, for which ϵ_K is equal to $k_B T_e$, known as the Einstein relation.

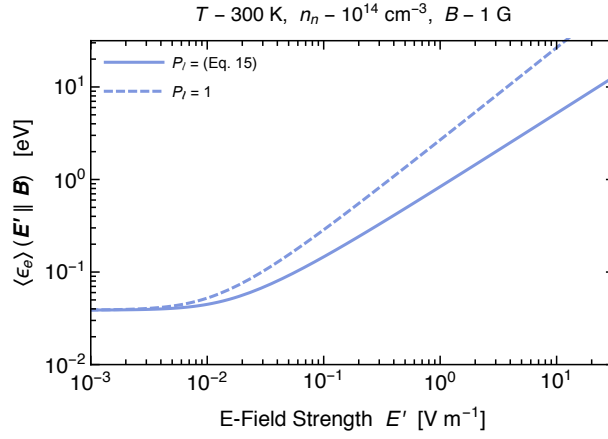


Figure 5. Electron mean energy $\langle \epsilon_e \rangle$ versus the electric field strength E' in the case of $E' \parallel B$ for the same parameters as in Figure 1. The solid line assumes P_ℓ given by Equation (15), while the dashed line shows how $\langle \epsilon_e \rangle$ would behave if all inelastic energy losses were absent, i.e., $P_\ell = 1$.

distribution function given by Equation (7) can be written as (Spitzer 1941; Shukla & Mamun 2002)

$$K_{de} = \pi a^2 \langle v_e \rangle \exp\left(-\frac{e^2 |Z|}{ak_B T_e}\right), \quad (\text{B2})$$

where $\langle v_e \rangle$ is the mean electron speed given by Equation (9). Equation (B2) assumes that the grains in the plasmas on average charge negatively, i.e., $Z < 0$, which is true as long as photoelectric and secondary electron emission from the grains are negligible (e.g., Shukla & Mamun 2002). Under this approximation, the Coulomb reduction factor C_e has a simple expression,

$$C_e \equiv \frac{K_{de}}{\pi a^2 \langle v_e \rangle} = \exp\left(-\frac{e^2 |Z|}{ak_B T_e}\right). \quad (\text{B3})$$

Note that $C_e < 0$.

The ion adsorption rate coefficient under the Maxwellian approximation can be written as (Shukla & Mamun 2002, Equation (46) of Paper I)

$$K_{di} = \pi a^2 \left[\sqrt{\frac{2k_B T_i}{\pi m_i}} \exp\left(-\frac{m_i \langle v_i \rangle^2}{2k_B T_i}\right) + |\langle v_i \rangle| \left(1 + \frac{k_B T_i + 2e^2 |Z|/a}{m_i \langle v_i \rangle^2}\right) \text{erf}\left(\sqrt{\frac{m_i}{2k_B T_i}} |\langle v_i \rangle|\right) \right], \quad (\text{B4})$$

where $\text{erfc}(x)$ is the complementary error function. The Coulomb attraction factor C_i can formally be defined as

$$C_i \equiv \frac{K_{di}}{\pi a^2 \langle v_i \rangle}, \quad (\text{B5})$$

with the mean ion speed $\langle v_i \rangle$ given by

$$\langle v_i \rangle = \sqrt{\frac{2k_B T_i}{\pi m_i}} \exp\left(-\frac{m_i \langle v_i \rangle^2}{2k_B T_i}\right) + |\langle v_i \rangle| \left(1 + \frac{k_B T_i}{m_i \langle v_i \rangle^2}\right) \text{erf}\left(\sqrt{\frac{m_i}{2k_B T_i}} |\langle v_i \rangle|\right), \quad (\text{B6})$$

which follows from the fact that K_{di} must have the form $K_{di} = \pi a^2 \langle v_i \rangle$ in the case of $Z = 0$. For $E' \gg E_{\text{crit},i}$, $\langle v_i \rangle$ and C_i have simple forms (Shukla & Mamun 2002, Equation (47) of Paper I)

$$\langle v_i \rangle \approx |\langle v_i \rangle|, \quad C_i \approx 1 + \frac{2e^2 |Z|}{am_i \langle v_i \rangle^2}. \quad (\text{B7})$$

The gas-phase recombination rate coefficient is taken as

$$K_{\text{rec}} = 2.4 \times 10^{-7} \left(\frac{T_e}{300 \text{ K}} \right)^{-0.69} \text{ cm}^3 \text{ s}^{-1}, \quad (\text{B8})$$

which assumes that the dominant positive ion is HCO^+ (Ganguli et al. 1988).

REFERENCES

- Bai, X.-N. 2011, *ApJ*, 739, 50, doi: [10.1088/0004-637X/739/1/50](https://doi.org/10.1088/0004-637X/739/1/50)
 —. 2014, *ApJ*, 791, 137, doi: [10.1088/0004-637X/791/2/137](https://doi.org/10.1088/0004-637X/791/2/137)
 —. 2015, *ApJ*, 798, 84, doi: [10.1088/0004-637X/798/2/84](https://doi.org/10.1088/0004-637X/798/2/84)
 —. 2017, *ApJ*, 845, 75, doi: [10.3847/1538-4357/aa7dda](https://doi.org/10.3847/1538-4357/aa7dda)
 Bai, X.-N., & Goodman, J. 2009, *ApJ*, 701, 737, doi: [10.1088/0004-637X/701/1/737](https://doi.org/10.1088/0004-637X/701/1/737)
 Bai, X.-N., & Stone, J. M. 2013a, *ApJ*, 767, 30, doi: [10.1088/0004-637X/767/1/30](https://doi.org/10.1088/0004-637X/767/1/30)
 —. 2013b, *ApJ*, 769, 76, doi: [10.1088/0004-637X/769/1/76](https://doi.org/10.1088/0004-637X/769/1/76)
 Balbus, S. A., & Hawley, J. F. 1991, *ApJ*, 376, 214, doi: [10.1086/170270](https://doi.org/10.1086/170270)
 Béthune, W., Lesur, G., & Ferreira, J. 2017, *A&A*, 600, A75, doi: [10.1051/0004-6361/201630056](https://doi.org/10.1051/0004-6361/201630056)
 Cleeves, L. I., Adams, F. C., Bergin, E. A., & Visser, R. 2013, *ApJ*, 777, 28, doi: [10.1088/0004-637X/777/1/28](https://doi.org/10.1088/0004-637X/777/1/28)
 Davydov, B. 1935, *Phys. Z. Sowjet.*, 8, 59
 Desch, S. J., & Cuzzi, J. N. 2000, *Icarus*, 143, 87, doi: [10.1006/icar.1999.6245](https://doi.org/10.1006/icar.1999.6245)
 Engelhardt, A. G., & Phelps, A. V. 1963, *Physical Review*, 131, 2115, doi: [10.1103/PhysRev.131.2115](https://doi.org/10.1103/PhysRev.131.2115)
 Gammie, C. F. 1996, *ApJ*, 457, 355, doi: [10.1086/176735](https://doi.org/10.1086/176735)
 Ganguli, B., Biondi, M. A., Johnsen, R., & Dulane, J. L. 1988, *PhRvA*, 37, 2543, doi: [10.1103/PhysRevA.37.2543](https://doi.org/10.1103/PhysRevA.37.2543)
 Golant, V. E., Zhilinsky, A. P., & Sakharov, I. E. 1980, *Fundamentals of plasma physics* (Wiley New York)
 Gressel, O., Turner, N. J., Nelson, R. P., & McNally, C. P. 2015, *ApJ*, 801, 84, doi: [10.1088/0004-637X/801/2/84](https://doi.org/10.1088/0004-637X/801/2/84)
 Hayashi, C. 1981, *Progress of Theoretical Physics Supplement*, 70, 35, doi: [10.1143/PTPS.70.35](https://doi.org/10.1143/PTPS.70.35)
 Hershey, A. V. 1939, *Physical Review*, 56, 916, doi: [10.1103/PhysRev.56.916](https://doi.org/10.1103/PhysRev.56.916)
 Ilgner, M., & Nelson, R. P. 2006, *A&A*, 445, 205, doi: [10.1051/0004-6361:20053678](https://doi.org/10.1051/0004-6361:20053678)
 Inutsuka, S., & Sano, T. 2005, *ApJL*, 628, L155, doi: [10.1086/432796](https://doi.org/10.1086/432796)
 Johansen, A., & Okuzumi, S. 2018, *A&A*, 609, A31, doi: [10.1051/0004-6361/201630047](https://doi.org/10.1051/0004-6361/201630047)
 Kunz, M. W. 2008, *MNRAS*, 385, 1494, doi: [10.1111/j.1365-2966.2008.12928.x](https://doi.org/10.1111/j.1365-2966.2008.12928.x)
 Kunz, M. W., & Balbus, S. A. 2004, *MNRAS*, 348, 355, doi: [10.1111/j.1365-2966.2004.07383.x](https://doi.org/10.1111/j.1365-2966.2004.07383.x)
 Kunz, M. W., & Lesur, G. 2013, *MNRAS*, 434, 2295, doi: [10.1093/mnras/stt1171](https://doi.org/10.1093/mnras/stt1171)
 Lesur, G., Kunz, M. W., & Fromang, S. 2014, *A&A*, 566, A56, doi: [10.1051/0004-6361/201423660](https://doi.org/10.1051/0004-6361/201423660)
 Mori, S., Bai, X.-N., & Okuzumi, S. 2019, *ApJ*, 872, 98, doi: [10.3847/1538-4357/ab0022](https://doi.org/10.3847/1538-4357/ab0022)
 Mori, S., Muranushi, T., Okuzumi, S., & Inutsuka, S.-i. 2017, *ApJ*, 849, 86, doi: [10.3847/1538-4357/aa8e42](https://doi.org/10.3847/1538-4357/aa8e42)
 Mori, S., & Okuzumi, S. 2016, *ApJ*, 817, 52, doi: [10.3847/0004-637X/817/1/52](https://doi.org/10.3847/0004-637X/817/1/52)
 Muranushi, T., Okuzumi, S., & Inutsuka, S. 2012, *ApJ*, 760, 56, doi: [10.1088/0004-637X/760/1/56](https://doi.org/10.1088/0004-637X/760/1/56)
 Nakano, T., & Umebayashi, T. 1986, *MNRAS*, 218, 663
 Okuzumi, S. 2009, *ApJ*, 698, 1122, doi: [10.1088/0004-637X/698/2/1122](https://doi.org/10.1088/0004-637X/698/2/1122)
 Okuzumi, S., & Inutsuka, S.-i. 2015, *ApJ*, 800, 47, doi: [10.1088/0004-637X/800/1/47](https://doi.org/10.1088/0004-637X/800/1/47)
 Sano, T., Miyama, S. M., Umebayashi, T., & Nakano, T. 2000, *ApJ*, 543, 486, doi: [10.1086/317075](https://doi.org/10.1086/317075)
 Shukla, P. K., & Mamun, A. A. 2002, *Introduction to dusty plasma physics*
 Simon, J. B., Bai, X.-N., Armitage, P. J., Stone, J. M., & Beckwith, K. 2013a, *ApJ*, 775, 73, doi: [10.1088/0004-637X/775/1/73](https://doi.org/10.1088/0004-637X/775/1/73)
 Simon, J. B., Bai, X.-N., Stone, J. M., Armitage, P. J., & Beckwith, K. 2013b, *ApJ*, 764, 66, doi: [10.1088/0004-637X/764/1/66](https://doi.org/10.1088/0004-637X/764/1/66)
 Spitzer, Jr., L. 1941, *ApJ*, 93, 369, doi: [10.1086/144273](https://doi.org/10.1086/144273)
 Stepinski, T. F. 1992, *Icarus*, 97, 130, doi: [10.1016/0019-1035\(92\)90062-C](https://doi.org/10.1016/0019-1035(92)90062-C)
 Turner, N. J., Fromang, S., Gammie, C., et al. 2014, *Protostars and Planets VI*, 411, doi: [10.2458/azu_uapress.9780816531240-ch018](https://doi.org/10.2458/azu_uapress.9780816531240-ch018)
 Umebayashi, T., & Nakano, T. 1981, *PASJ*, 33, 617
 —. 2009, *ApJ*, 690, 69, doi: [10.1088/0004-637X/690/1/69](https://doi.org/10.1088/0004-637X/690/1/69)
 Wannier, G. H. 1953, *Bell System Technical Journal*, 32, 170
 Wardle, M. 2007, *Ap&SS*, 311, 35, doi: [10.1007/s10509-007-9575-8](https://doi.org/10.1007/s10509-007-9575-8)
 Wardle, M., & Ng, C. 1999, *MNRAS*, 303, 239, doi: [10.1046/j.1365-8711.1999.02211.x](https://doi.org/10.1046/j.1365-8711.1999.02211.x)
 Wardle, M., & Salmeron, R. 2012, *MNRAS*, 422, 2737, doi: [10.1111/j.1365-2966.2011.20022.x](https://doi.org/10.1111/j.1365-2966.2011.20022.x)
 Weidenschilling, S. J. 1977, *Ap&SS*, 51, 153, doi: [10.1007/BF00642464](https://doi.org/10.1007/BF00642464)

Whipple, F. L. 1966, *Science*, 153, 54,

doi: [10.1126/science.153.3731.54](https://doi.org/10.1126/science.153.3731.54)

Xu, R., & Bai, X.-N. 2016, *ApJ*, 819, 68,

doi: [10.3847/0004-637X/819/1/68](https://doi.org/10.3847/0004-637X/819/1/68)

Yoon, J.-S., Song, M.-Y., Han, J.-M., et al. 2008, *Journal of Physical and Chemical Reference Data*, 37, 913,

doi: [10.1063/1.2838023](https://doi.org/10.1063/1.2838023)